

Effects of Zeroline and Ferrimagnetic Fluctuation on Nuclear Magnetic Resonance for Dirac Electrons in Molecular Conductor α -(BEDT-TTF)₂I₃

A. Kobayashi, Y. Suzumura

Department of Physics, Nagoya University, Furo-cho, Chikusa-ku, Nagoya, 464-8602 Japan

(Dated: November 26, 2018)

We re-examine the wave function of two-dimensional massless Dirac electron in α -(BEDT-TTF)₂I₃ consisting of four molecules A, A', B and C in a unit cell, using a tight-binding model. We find zerolines in the Brillouin zone, on which the component of the wave function becomes zero for B or C sites. The zerolines, which are bounded by two Dirac points at $\pm\mathbf{k}_0$ and pass through the M- or Y-points, result in a fact that the density of states of the B site exhibits no the Van Hove singularity near the energy of the Dirac points. By taking account of the on-site Coulomb interaction within the random phase approximation, we examine the spin fluctuation in order to investigate properties of the nuclear magnetic resonance for temperatures $T > 50\text{K}$. In the region for $100 < T < 300\text{K}$, it is shown that the Knight shift for B-site monotonously decreases with decreasing temperature, owing to lack of the Van Hove singularity, while it shows a maximum for the other sites (A, A' and C sites). In the region for $50 < T < 100\text{K}$, it is shown that the Knight shift is convex downward and the Korringa ratio increases with decreasing temperature for B-site. Such a behavior originates from the ferrimagnetic spin fluctuation related to the zerolines. These results are consistent with those of the nuclear magnetic resonance experiments.

I. INTRODUCTION

Molecular conductor α -(BEDT-TTF)₂I₃¹ has highly two-dimensional electronic system in the plane of BEDT-TTF^{1/2} molecule owing to layered structure with the plane of I₃⁻ anion, and has brought much interest by the variety of electronic states, such as a charge ordered state², a superconducting state in the presence of charge ordering, and a zero gap state (ZGS) with a massless Dirac electron³.

The charge ordered state was suggested theoretically using an extended Hubbard model⁴⁻⁶, and was confirmed by NMR experiment⁷. The superconducting state with the charge ordering under uniaxial pressure along the stacking axis (*a*-axis)⁸ was also investigated theoretically using the extended Hubbard model⁹. A narrow gap state (NGS) was suggested to explain both anomalous increase of Hall coefficient and almost-constant resistivity with decreasing temperature at high pressures¹⁰. From the calculation of the NGS, it was obtained that the charge gap disappears at high pressure, leading to the density of state (DOS) vanishing linearly at the Fermi energy¹¹. Further, the ZGS with a Dirac cone in energy dispersion was found theoretically¹² using the transfer energies of ref. 13, and was also confirmed by the first principle calculations^{14,15}. The energy spectrum near the Fermi energy exhibits two tilted Dirac cones, which are described by the tilted Weyl equation^{16,17}. The tilt of the Dirac cone has been confirmed by a comparison between the theoretical and experimental results for the temperature (*T*) dependence of the Hall coefficient^{18,19} and the angular dependence of the magnetoresistance^{19,20}. From the calculation of the variation of the Dirac point, the emergence of a pair of massive Dirac points is predicted in the charge ordering state at low pressures²¹, the merging of two massless Dirac electrons is shown at extremely

high pressures¹⁶, suggesting robustness of Dirac electrons against uniaxial pressures. Effects of electron correlation for long range Coulomb repulsion in the tilted Dirac electron system have been investigated theoretically in the absence of magnetic field^{22,23} and in the presence of magnetic field²⁴. As for the short range part of Coulomb repulsion, on the other hand, effect of fluctuations in ZGS has not yet investigated theoretically in the context of inequivalence of BEDT-TTF sites ($A = A' \neq B \neq C$ as shown in Fig. 1).

The property of the wave function plays important roles in the DOS and the electron-hole excitation in α -(BEDT-TTF)₂I₃. The anomalous behavior of the Bloch wave functions exists in the vicinity of the Dirac point. The momentum dependences of the velocity matrix and the charge density exhibit a singularity at the point.¹⁶ The angular dependence of the wave functions for each site reveals a fact that the absolute value becomes zero for B site or C site at a special direction of the point²⁸. The theoretical calculation of Knight shift K_α and $(1/T_1T)_\alpha$ ²⁸. has been performed based on a tight-binding model for α -(BEDT-TTF)₂I₃ where $K_\alpha \propto T$ and $(1/T_1T)_\alpha \propto T^2$ owing to the Dirac cone spectrum. The Knight shift for the respective site reveals a relation, $K_C > K_A > K_B$, which is consistent with experimental results,²⁵ originates from both the tilt of Dirac cone and property of wave function in the vicinity of the Dirac point. Thus, the inequivalence of BEDT-TTF sites observed in NMR experiments reveals inner degree of freedom of Dirac electron in molecular conductors.²⁵⁻²⁷

However, the tight binding model is not enough to explain the details, e.g, the non-linear temperature dependences of K_α as shown in the following experiment. In high temperature region ($T > 100\text{K}$), the Knight shift K_α with decreasing temperature monotonously decreases for $\alpha = \text{B}$ site, while it exhibits a maximum

for $\alpha = A$ and C sites. In medium temperature region ($50 < T < 100\text{K}$), the Knight shift is convex downward with decreasing temperature for B site, while the components for A and C sites exhibit linear T -dependences.^{25,27} For a local NMR relaxation rate $1/T_1$, the difference in $(1/T_1 T)_\alpha$ in $\alpha = A, B,$ and C sites, is small in low temperature region ($T < 50\text{K}$), i.e., all components are convex downward with T^2 -dependences for $T < 100\text{K}$. As a result, the Korringa ratio $(1/T_1 T K^2)_\alpha$ for $\alpha = B$ site clearly increases with decreasing T in medium temperature region, and exhibits an inequality $(1/T_1 T K^2)_B > (1/T_1 T K^2)_A > (1/T_1 T K^2)_C$ ²⁷.

In the present paper, we re-examine the wave function in α -(BEDT-TTF)₂I₃ using a tight-binding model where the transfer integrals are given by the first principle calculation¹⁴, and calculate the spin fluctuation within the random phase approximation on the on-site Coulomb interaction to investigate K_α and $(1/T_1 T)_\alpha$ for $T > 50\text{K}$. Based on the formulation in §II, we demonstrate following new results in §III. We find zerolines in the two-dimensional Brillouin zone, where the wave function is zero for the components of B or C site. They are bounded by the two Dirac points at $\pm\mathbf{k}_0$. The zerolines passing through the M - or Y -points give rise to the absence of two Van Hove singularities for only the B -site. In the high temperature region for $100 < T < 300\text{K}$, the present numerical results on T -dependences of K_α , are consistent with the experimental results²⁵⁻²⁷, where existence (absence) of Van Hove singularities for $\alpha = A$ and C sites ($\alpha = B$ site) is essential. In the region for $50 < T < 100\text{K}$, it is shown that K_B is convex downward, $(1/T_1 T K^2)_B$ increases with decreasing T , and then the inequality $(1/T_1 T K^2)_B > (1/T_1 T K^2)_A > (1/T_1 T K^2)_C$ is reproduced, owing to the ferrimagnetic spin fluctuation related to the zerolines and enhanced by the on-site Coulomb interaction. These results are also consistent with those experimental results²⁵⁻²⁷. In §IV, summary and discussion are given.

II. FORMULATION

The model describing the two-dimensional electronic system in α -(BEDT-TTF)₂I₃ is shown in Fig. 1^{14,29,30}. The unit cell consists of four BEDT-TTF molecules on sites A, A', B and C , where A is equivalent to A' so that inversion symmetry is preserved, while the sites A, B and C are inequivalent. There are six electrons for the four molecules in a unit cell, thus the bands are $3/4$ -filled. On the basis of the HOMO orbitals of these sites^{4,5}, these electrons are described by a Hubbard model with the on-site Coulomb interaction U ,

$$H = \sum_{(i\alpha;j\beta),\sigma} (t_{i\alpha;j\beta} a_{i\alpha\sigma}^\dagger a_{j\beta\sigma} + \text{h.c.}) + \sum_{i\alpha} U a_{i\alpha\uparrow}^\dagger a_{i\alpha\downarrow}^\dagger a_{i\alpha\downarrow} a_{i\alpha\uparrow}, \quad (2.1)$$

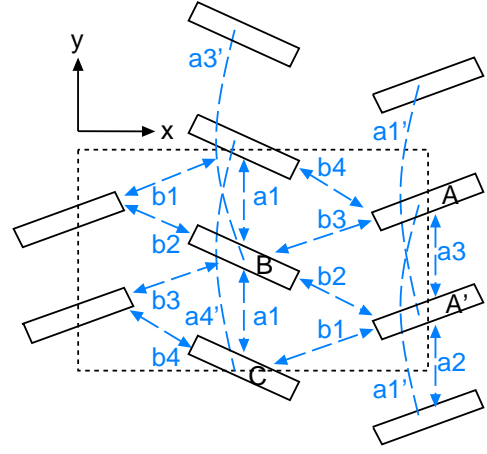


FIG. 1: The model describing the electronic system of α -(BEDT-TTF)₂I₃^{14,29,30}. The unit cell consists of four BEDT-TTF molecules A, A', B and C with ten transfer energies. The a - and b -axis in the conventional notation correspond to the y - and x -axis in the present paper. The molecules A and A' are equivalent in the presence of the inversion symmetry in the ZGS. (Color Online)

where i, j denote indices of a given unit cell, and $\alpha, \beta (= A, A', B$ and $C)$ are indices of BEDT-TTF sites in the unit cell. In the first term, $a_{i\alpha\sigma}^\dagger$ denotes a creation operator with spin $\sigma (= \uparrow, \downarrow)$ and $t_{i\alpha;j\beta}$ is the transfer energy between the (i, α) site and the (j, β) site. Throughout the paper, \hbar and the lattice constant a are taken as unity. Hereafter, the energies are given in eV, and the temperature is also given by $k_B T$ in eV, i. e. $1\text{eV} = 10^4\text{K}$, where k_B is the Boltzmann factor.

The transfer energies at finite temperature T is estimated by the interpolation formula²⁸

$$t_X(T) = t_X(\text{LT}) + (t_X(\text{RT}) - t_X(\text{LT}))(T - \text{LT}) / (\text{RT} - \text{LT}). \quad (2.2)$$

The transfer energies $t_X(\text{RT})$ and $t_X(\text{LT})$ are given by the 1st principle calculation¹⁴, where $t_{a1}(\text{RT}) = -0.0101, t_{a2}(\text{RT}) = -0.0476, t_{a3}(\text{RT}) = 0.0093, t_{b1}(\text{RT}) = 0.1081, t_{b2}(\text{RT}) = 0.1109, t_{b3}(\text{RT}) = 0.0551, t_{b4}(\text{RT}) = 0.0151, t_{a1'}(\text{RT}) = 0.0088, t_{a3'}(\text{RT}) = 0.0019, t_{a4'}(\text{RT}) = 0.0009,$ and $t_{a1}(\text{LT}) = -0.0267, t_{a2}(\text{LT}) = -0.0511, t_{a3}(\text{LT}) = 0.0323, t_{b1}(\text{LT}) = 0.1241, t_{b2}(\text{LT}) = 0.1296, t_{b3}(\text{LT}) = 0.0513, t_{b4}(\text{LT}) = 0.0512, t_{a1'}(\text{LT}) = 0.0119, t_{a3'}(\text{LT}) = 0.0046, t_{a4'}(\text{LT}) = 0.0060,$, where low temperature $\text{LT} = 0.0008$ and we put room temperature $\text{RT} = 0.03$.

The Hamiltonian is diagonalized numerically for a given \mathbf{k} in each spin subspace, according to

$$\sum_{\beta=1}^4 \tilde{\epsilon}_{\alpha\beta\sigma}(\mathbf{k}) d_{\beta\gamma\sigma}(\mathbf{k}) = \xi_{\gamma\sigma}(\mathbf{k}) d_{\alpha\gamma\sigma}(\mathbf{k}), \quad (2.3)$$

where $\xi_{\gamma\sigma}$ are the eigenenergies ordered such that, $\xi_{1\sigma}(\mathbf{k}) > \xi_{2\sigma}(\mathbf{k}) > \xi_{3\sigma}(\mathbf{k}) > \xi_{4\sigma}(\mathbf{k})$ ($\gamma = 1, 2, 3, 4$ is the

band index), and $d_{\alpha\gamma\sigma}(\mathbf{k})$ are the corresponding eigenvectors. The T -dependence of the chemical potential owing to the electron-hole asymmetry¹⁸ is taken into account in the present calculation, although it has not been considered in 28.

The bare susceptibility on the site representation is given by¹¹

$$\begin{aligned} [\hat{\chi}^0]_{\alpha\beta} &= \chi_{\alpha\beta}^0(\mathbf{q}, \omega_l) \\ &= -\frac{T}{N_L} \sum_{\mathbf{kn}} G_{\alpha\beta}(\mathbf{k} + \mathbf{q}, \epsilon_n + \omega_l) G_{\beta\alpha}(\mathbf{k}, \epsilon_n) \quad (2.4) \\ &= -\frac{T}{N_L} \sum_{\mathbf{kn}} \frac{F_{\alpha\beta}(\mathbf{k}, \mathbf{q})}{(i(\epsilon_n + \omega_l) - \xi_\gamma(\mathbf{k} + \mathbf{q}))(i\epsilon_n - \xi_\gamma(\mathbf{k}))} \quad (2.5) \end{aligned}$$

where the bare Green function on the site representation is defined by

$$G_{\alpha\beta}(\mathbf{k}, \epsilon_n) \equiv \sum_{\gamma} d_{\alpha\gamma}(\mathbf{k}) d_{\beta\gamma}^*(\mathbf{k}) / (i\epsilon_n - \xi_\gamma(\mathbf{k})) \quad (2.6)$$

with $\epsilon_n = (2n + 1)\pi T$ and $\omega_l = 2n\pi T$ are the Matsubara frequencies, and the form factor is defined by

$$F_{\alpha\beta}(\mathbf{k}, \mathbf{q}) = F_{\alpha\beta}^{(1)}(\mathbf{k}, \mathbf{q}) + F_{\alpha\beta}^{(2)}(\mathbf{k}, \mathbf{q}), \quad (2.7)$$

$$F_{\alpha\beta}^{(1)}(\mathbf{k}, \mathbf{q}) = \sum_{\gamma=1,2} F_{\alpha\beta}^{\gamma\gamma}(\mathbf{k}, \mathbf{q}), \quad (2.8)$$

$$F_{\alpha\beta}^{(2)}(\mathbf{k}, \mathbf{q}) = \sum_{\gamma=1,2} F_{\alpha\beta}^{\gamma\bar{\gamma}}(\mathbf{k}, \mathbf{q}), \quad (2.9)$$

$$F_{\alpha\beta}^{\gamma\bar{\gamma}'}(\mathbf{k}, \mathbf{q}) = d_{\alpha\gamma}(\mathbf{k} + \mathbf{q}) d_{\beta\gamma}(\mathbf{k} + \mathbf{q})^* d_{\beta\bar{\gamma}'}(\mathbf{k}) d_{\alpha\bar{\gamma}'}(\mathbf{k})^*, \quad (2.10)$$

with $\bar{\gamma} \neq \gamma$ indicating another band within the conduction ($\gamma = 1$) and valence ($\gamma = 2$) bands. The form factor reflects the character of each site for the intraband ($F_{\alpha\beta}^{(1)}(\mathbf{k}, \mathbf{q})$) and interband ($F_{\alpha\beta}^{(2)}(\mathbf{k}, \mathbf{q})$) fluctuations.

In the presence of spin symmetry, the longitudinal spin susceptibility, $\hat{\chi}^s$, and the transverse spin susceptibility, $\hat{\chi}^\pm$, are given by¹¹

$$\hat{\chi}^s = \hat{\chi}^\pm = (1 - \hat{\chi}^0 \hat{U})^{-1} \hat{\chi}^0 \quad (2.11)$$

with $\hat{U} = U\hat{I}$ and \hat{I} is the unit matrix.

The knight shift K_α (the local spin susceptibility) and the local NMR relaxation rate $(1/T_1)_\alpha$ with A, A', B and C sites are given by²⁸

$$K_\alpha = \sum_{\beta} \chi_{\alpha\beta}^s(\mathbf{0}, 0), \quad (2.12)$$

$$(1/T_1)_\alpha = T \lim_{\omega \rightarrow 0} \sum_{\mathbf{q}} \text{Im}[\chi_{\alpha\alpha}^\pm(\mathbf{q}, \omega)] / \omega. \quad (2.13)$$

III. RESULTS

A. Zeroline and density of states

Figure 2(a), (b), (c) and (d) show absolute values of the wave functions of the conduction band ($\gamma = 1$) for

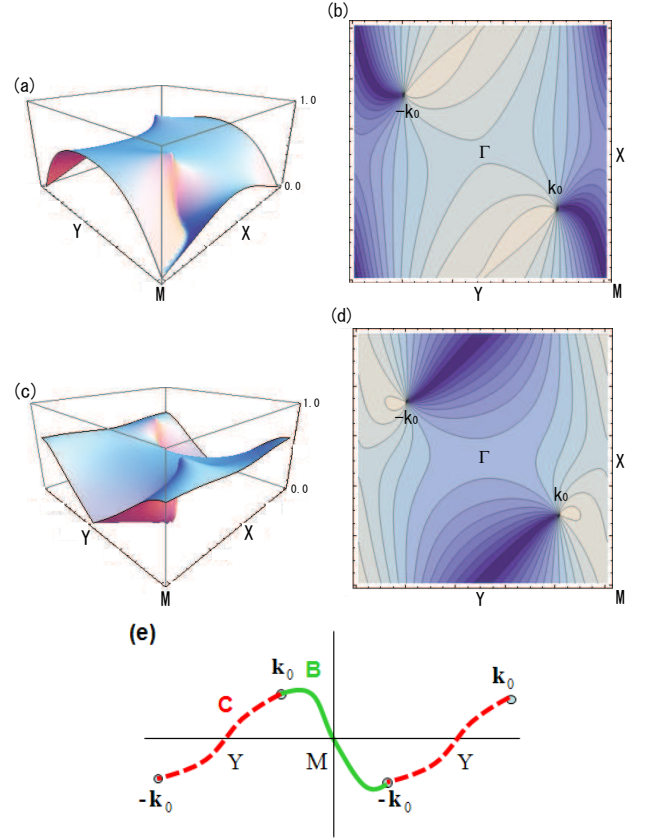


FIG. 2: Absolute values of the wave functions of the conduction band ($\xi = 1$) for the components of B site ($|d_{B1}(\mathbf{k})d_{B1}^*(\mathbf{k})|$ (a)) and their contour plot(b)) and those of C site ((c) and (d)) in the Brillouin zone. The zerolines of the conduction band are bounded by two Dirac points at $\pm\mathbf{k}_0$ as shown in the dark region of (c) and (d), and in schematic figure (e) for B site (green solid line) and C site (red dashed line). (Color Online)

the components of B site (Figs 2(a) and (b)) and C site (Figs 2(c) and (d)). We find "zerolines" which are curved lines where absolute value of the wave function is zero, only for the components of B and C sites. The zerolines for both B and C sites are bounded by two Dirac points at $\pm\mathbf{k}_0$ in the Brillouin zone, where the wave functions are discontinuous. In the conduction band, the zeroline for B (C) site passes through the M - (Y -)point as shown in Fig 2(e). In the valence band, on the contrary, the zeroline for B (C) site passes through the Y - (M -)point. The zeroline for B (C) site in conduction band coincides with the zeroline for C (B) site in valence band in the vicinity of the Dirac points. , while these are slightly different far from the Dirac points, since the conduction and valence bands are not equivalent in α -type organic conductors.

In Fig 3(a), the conduction band and the valence band are shown. The chemical potential with $\omega = 0$ is situated on the Dirac points at $T = 0$, while it decreases with increasing temperature owing to the asymmetry of the

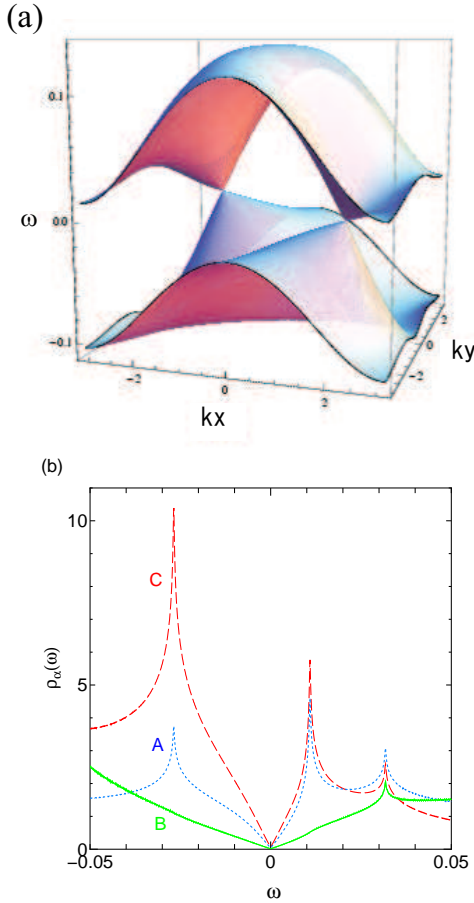


FIG. 3: (a) Energy dispersions in the Brillouin zone for the conduction and valence bands ($\gamma = 1$ and 2), which has a contact point with the tilted Dirac cones at $\pm \mathbf{k}_0$. The chemical potential is given by with $\omega = 0$. There are the saddle points at the M -point in the conduction band and at Y -point in the valence band near $\omega = 0$. (b) The density of states ρ_α near the energy of the Dirac point ($\omega = 0$) at $T = 0$ for the components of $\alpha = A$ site (blue dotted line), $\alpha = B$ site (green solid line), and $\alpha = C$ site (red dashed line). (Color Online)

conduction and valence bands.¹⁸ The saddle points close to the Fermi energy are seen at the M -point and at Y -point, respectively. The saddle points give rise to the Van Hove singularities $\omega = 0.012\text{eV}$ in the conduction band, and at $\omega = -0.026\text{eV}$ in the valence band. Such a singularity appears in the components of density of state at A and C sites as shown in Fig 3(b), where the energy of the Dirac points is $\omega = 0$. For the component of B site, however, these two Van Hove singularities disappear, since the zeroline for B site passes through the location of the saddle point.

B. Knight shift and NMR relaxation rate

Figure 4(a) shows temperature dependences of the Knight shift K_α for $\alpha = A, B$, and C sites with $U = 0.12$ and K_α^0 with $U = 0$. The value of $U = 0.12$ is chosen so that the temperature dependences of K_α in the present calculation reproduce those of experimental results for $T > 50\text{K}$. The Knight shift K_α^0 (with $U = 0$) for $T < 0.015$ has been calculated in ref. 28, which gives slightly different results due to ignoring the T -dependence of the chemical potential. In high temperature region ($100 < T < 300\text{K}$), With decreasing temperature, the Knight shift monotonously decreases for B -site while there is a maximum in the temperature dependence of the Knight shift for A and C sites. Such behavior is independent of U originates from the combined effect of the Van Hove singularity and the zerolines as discussed in Fig 3. In medium temperature region ($50 < T < 100\text{K}$), on the other hand, it is shown that the Knight shift is convex downward with decreasing temperature for B -site with $U = 0.12$, while the components for A and C sites exhibit linear T -dependences in this region. Such a effect of electron correlation originates from the ferrimagnetic spin fluctuation described later. Figure 4(b) shows temperature dependences of $(1/T_1T)_\alpha$ for $\alpha = A, B$, and C sites with $U = 0.12$ and $(1/T_1T)_\alpha^0$ with $U = 0$. It is shown that $(1/T_1T)_\alpha$ exhibit linear T^2 -dependences with $T < 100\text{K}$ approximately, and all components are weakly enhanced by U . Figure 4(c) shows temperature dependences of the Korringa ratio $(1/T_1TK^2)_\alpha$ for $\alpha = A, B$, and C sites with $U = 0.12$ and $(1/T_1TK^2)_\alpha^0$ with $U = 0$. It is clearly shown that the Korringa ratio for B site is strongly enhanced by U and increases with decreasing T , owing to the anomalous T -dependence of K_B . The electron correlation effect results in the enhancement of the following inequality,

$$(1/T_1TK^2)_B > (1/T_1TK^2)_A > (1/T_1TK^2)_C. \quad (3.1)$$

C. Ferrimagnetic fluctuation in spin susceptibility

We examine static spin susceptibility at low energy by choosing $T = 0.02$ and $\omega = 0$. In Fig 5(a), the momentum dependences of the diagonal components of the spin susceptibilities $\chi_{\alpha\alpha}^s$ and the bare susceptibilities $\chi_{\alpha\alpha}^0$ ($U = 0$) for $\alpha = A, B$, and C are shown for $\alpha = A, B$, and C with $U = 0.12$. The diagonal components are positive in the Brillouin zone and are enhanced by U . The momentum dependences of the off-diagonal components of the spin susceptibilities $\chi_{\alpha\beta}^s$ for $(\alpha, \beta) = (A, B)$, (B, C) , and (A, C) with $U = 0.12$, and the bare susceptibilities $\chi_{\alpha\beta}^0$ for $(\alpha, \beta) = (A, B)$, (B, C) , and (A, C) with $U = 0$ are shown in Fig 5(b). It is found that χ_{BC}^s and χ_{AB}^s are negative in the Brillouin zone, while χ_{AC}^s has both positive and negative value. Those absolute values are enhanced by U . Especially, χ_{BC}^s plays the most

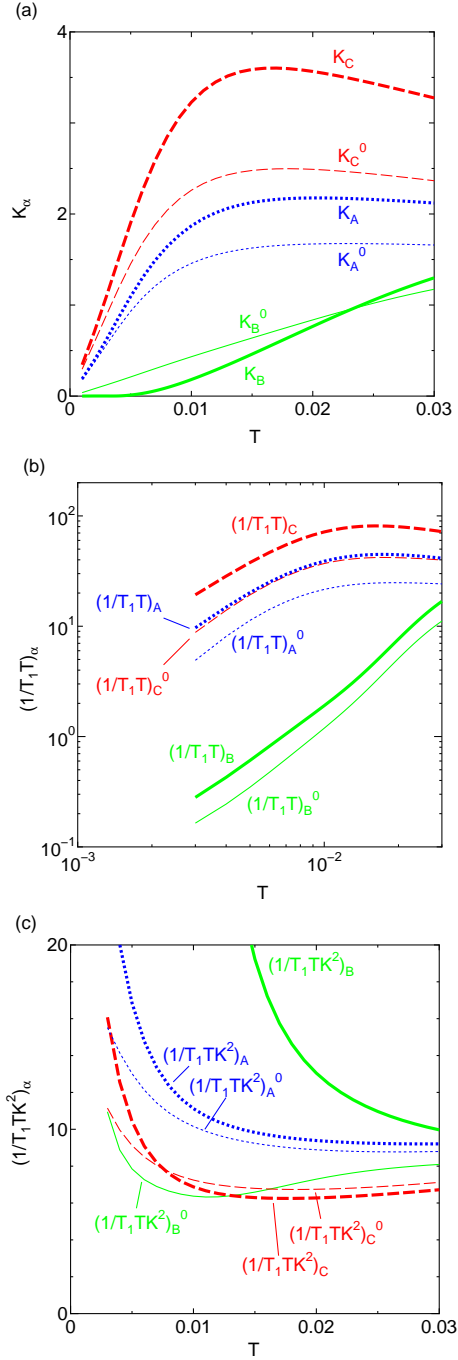


FIG. 4: (a) Temperature dependences of the Knight shift K_α with $U = 0.12$ (thick line) and K_α^0 (thin line) for $\alpha = A$ (red dashed line), B (green solid line), and C sites (blue dotted line), respectively. (b) Temperature dependences of $(1/T_1 T)_\alpha$ with $U = 0.12$ (thick line) and $(1/T_1 T)_\alpha^0$ (thin line) for $\alpha = A$ (red dashed line), B (green solid line), and C sites (blue dotted line), respectively. (c) Temperature dependences of Korringa ratio $(1/T_1 T K^2)_\alpha$ with $U = 0.12$ (thick line) and $(1/T_1 T K^2)_\alpha^0$ with $U = 0$ (thin line) for $\alpha = A$ (red dashed line), B (green solid line), and C sites (blue dotted line), respectively. (Color Online)

important role for the anomalous T -dependences of K_B , since $|\chi_{BC}^s|$ at $\mathbf{q} = \mathbf{0}$ is strongly enhanced by U , owing to product of negative χ_{BC}^0 with positive diagonal terms in the RPA process such as

$$[\hat{\chi}^s]_{BC} = [(1 - \hat{\chi}^0 \hat{U})^{-1} \hat{\chi}^0]_{BC} = \chi_{BC}^0 + U \chi_{BB}^0 \chi_{BC}^0 + U \chi_{BC}^0 \chi_{CC}^0 + \dots \quad (3.2)$$

Negative off-diagonal susceptibilities, χ_{BC}^s and χ_{AB}^s , and positive off-diagonal susceptibility, χ_{AC}^s , at $\mathbf{q} = \mathbf{0}$ indicate the ferrimagnetic spin fluctuation where the spin on B site tends to be opposite to that of the other sites as shown in Fig 5(c). The Knight shift is a sum of the diagonal and off-diagonal spin susceptibilities, where the former are dominant at high temperatures since the spin fluctuation exhibits local character. The latter become important with decreasing temperature, resulting in the anomalous T -dependence of K_B which is convex downward at low temperatures.

The negative value of χ_{BC}^0 at $\mathbf{q} = \mathbf{0}$ originates from the form factor for the interband fluctuation, $F_{BC}^{(2)}(\mathbf{k}, \mathbf{0})$, since the form factor for intraband fluctuation, $F_{BC}^{(1)}(\mathbf{k}, \mathbf{0})$, is positive for any \mathbf{k} . The momentum \mathbf{k} dependence of $F_{BC}^{(2)}(\mathbf{k}, \mathbf{0})$ in the Brillouin zone is shown in Figs 6(a) and 6(b). Although $F_{BC}^{(2)}(\mathbf{k}, \mathbf{0})$ can take positive or negative values, the numerical result show $F_{BC}^{(2)}(\mathbf{k}, \mathbf{0})$ is negative or zero for any \mathbf{k} . It is not a self-evident result owing to the phase structure of the wave function as discussed later. The white curved lines in Fig. 6(b) correspond to the zeroline for B and C sites, where $F_{BC}^{(2)}(\mathbf{k}, \mathbf{0}) = 0$.

In order to show the reason of $F_{BC}^{(2)}(\mathbf{k}, \mathbf{0}) \leq 0$, we investigate the phase structure of the wave function. Properties of wave functions in the vicinity of the Dirac points have been investigated by analyzing in terms of the Luttinger-Kohn representation²⁸. The analysis of wave functions in the present paper, on the other hand, is based on the Bloch representation. Figure 7 shows numerical results of wave functions for B and C sites and for conduction and valence bands, $d_{B1}(k_0')$, $d_{B2}(k_0')$, $d_{C1}(k_0')$ and $d_{C2}(k_0')$, on the Gauss plane, here $|k_0' - k_0| = 0.05\pi$, i.e., the momentum k_0' circles the Dirac point \mathbf{k}_0 . In order to avoid arbitrary phase factor of the wave functions for each band γ and each momentum k_0' , we choose $d_{A\gamma}(k_0')$ is real and positive. Such a representation for wave functions was used in ref. 32 to examine the rotation of the base, $d_{\alpha,1}$ and $d_{\alpha,2}$, around \mathbf{k}_0 . The inset shows θ -dependences of absolute values of the wave functions for the conduction band. The similar result was shown in 28 although there is slight difference in the choice of the horizontal axis. Based on this numerical results, the wave functions in the vicinity of the Dirac points, are approximately given by

$$\begin{aligned} d_{B1}(\theta) &= e^{i\theta_1} |d_{B1}| [e^{i(\theta+\theta_{B1})} - e^{i(\theta_{B2}+\theta_{B1})}], \\ d_{C1}(\theta) &= e^{i\theta_1} |d_{C1}| [e^{i(\theta+\theta_{C1})} - e^{i(\theta_{C2}+\theta_{C1})}], \\ d_{B2}(\theta) &= e^{i\theta_2} |d_{B2}| [e^{i(\theta+\theta_{B2})} - e^{i(\theta_{C2}+\theta_{B2})}], \end{aligned}$$

$$d_{C2}(\theta) = e^{i\theta_1} |d_{C2}| [e^{i(\theta+\theta_{C2})} - e^{i(\theta_{BZ}+\theta_{C2})}], \quad (3.3)$$

where θ is the angle of the vector $\mathbf{k}' - \mathbf{k}_0$ measured from k_x -axis. The values of wave functions at $\theta = 0$ are determined by θ_{B1} , θ_{C1} , θ_{B2} and θ_{C2} . The angle of the zeroline for B (C) site in the conduction band is θ_{BZ} (θ_{CZ}), where $|d_{B1}(\theta)| = 0$ ($|d_{C1}(\theta)| = 0$) as shown in the inset of Fig. 7, while the zeroline for B (C) site in the valence band corresponds to θ_{CZ} (θ_{BZ}). The arbitrary phases of the wave functions for each band and each momentum, $\theta_1(\theta)$ and $\theta_2(\theta)$, disappear in the form factor. Using above wave functions with the parameters given by the numerical calculation, we obtain $F_{BC}^{(2)}(\mathbf{k}^0, \mathbf{0}) \leq 0$ at arbitrary θ .

If $\theta_{CZ} = \theta_{BZ} + \pi$ (close to the present numerical result),

$$F_{BC}^{(2)}(\mathbf{k}^0, \mathbf{0}) = -8 \cos \theta_0 \sin^2(\theta - \theta_{BZ}) \quad (3.4)$$

with $\theta_0 = -\theta_{B1} + \theta_{C1} - \theta_{C2} + \theta_{B2}$. We obtain $F_{BC}^{(2)}(\mathbf{k}^0, \mathbf{0}) \leq 0$ in the wide region of parameter, $-\pi/2 \leq \theta_0 \leq \pi/2$. Thus the condition of $F_{BC}^{(2)}(\mathbf{k}^0, \mathbf{0}) \leq 0$ is robust when the zerolines of B and C sites extend in opposite directions each other. When $\theta_{CZ} = \theta_{BZ}$, on the other hand,

$$F_{BC}^{(2)}(\mathbf{k}^0, \mathbf{0}) = 8 \cos \theta_0 (1 - \cos(\theta - \theta_{BZ}))^2. \quad (3.5)$$

We obtain $F_{BC}^{(2)}(\mathbf{k}^0, \mathbf{0}) \leq 0$ with θ_0 in the present numerical result. Thus the angle between the zerolines of B and C sites is an important factor for the ferrimagnetic fluctuation in the Dirac electrons of α -(BEDT-TTF)₂I₃.

IV. SUMMARY AND DISCUSSION

In summary, we examined the wave function and the spin fluctuation in α -(BEDT-TTF)₂I₃, using a tight-binding model and the on-site Coulomb interaction treated within the random phase approximation. The effect of electron correlation on K_α and $(1/T_1T)_\alpha$ with A, A', B and C sites for $T > 50\text{K}$ was investigated paying attention to the inequivalence of these sites ($A = A' \neq B \neq C$).

We found that zerolines, where the wave function is zero for the components of B or C site. They give the vanishing of two Van Hove singularities near the energy of the Dirac points only for B-site component of DOS. Existence (absence) of the Van Hove singularities plays essential role for the T -dependences of K_α . For the high temperature region of $100 < T < 300\text{K}$, with decreasing T , K_B decreases monotonously while K_A and K_C exhibit a maximum. In the region for $50 < T < 100\text{K}$, K_B is convex downward, and $(1/T_1TK^2)_B$ increases leading to an inequality of the Korringa ratio, $(1/T_1TK^2)_B > (1/T_1TK^2)_A > (1/T_1TK^2)_C$, was obtained. These results are consistent with those of experiment for $T > 50\text{K}$ ²⁵⁻²⁷.

It is found that the anomalous T -dependence of K_B is ascribed to the ferrimagnetic spin fluctuation which is enhanced by the on-site Coulomb interaction. Such a fluctuation describes a spin on B site being opposite to the other spins on A, A' and C sites. The ferrimagnetic spin fluctuation originates from the interband fluctuation mainly between B and C sites. The interband fluctuation relates to the zerolines bounded by two Dirac points in the Brillouin zone. Such zeroline does not exist in the wave function of graphene, since carbon atoms in two sublattice are equivalent owing to the inversion symmetry, which corresponds to A and A' sites in α -(BEDT-TTF)₂I₃. Thus the present results reveal that the inequivalence of BEDT-TTF sites play important roles for observables in NMR as an inner degree of freedom of Dirac electron in molecular conductor with the short range Coulomb interaction.

There remain problems to be clarified. In the low temperature region for $T < 50$, K_α for all components are convex downward with decreasing T ²⁵⁻²⁷, and $(1/T_1T)_\alpha$ exhibits complex T -dependence for very low temperatures^{27,31} in the presence of magnetic field perpendicular to the conducting plane. Those behavior can not be explained within the random phase approximation on the on-site Coulomb interaction. It indicates an importance of a higher order correction such as self-energy correction with the long range Coulomb interaction, since at low temperatures, low energy phenomena in the vicinity of Dirac point is dominant and then scale of length is much longer than lattice constant. Finally, we note that the valley splitting owing to the pseudo-spin XY ferromagnetism in $N = 0$ Landau states²⁴ may also play significant roles at very low temperatures in the presence of magnetic field perpendicular to the conducting plane.

Acknowledgments

The authors are thankful to K. Ishikawa, M. Hirata, K. Miyagawa and K. Kanoda for fruitful discussions. Y.S. is indebted to the Daiko Foundation for financial aid in the present work. This work was financially supported in part by Grant-in-Aid for Special Coordination Funds for Promoting Science and Technology (SCF), Scientific Research on Innovative Areas 20110002, and was also financially supported by a Grant-in-Aid for Special Coordination Funds for Promoting Science and Technology (SCF) from the Ministry of Education, Culture, Sports, Science and Technology in Japan, and Scientific Research 19740205, 22540366, 23540403 and 24244053 from the Ministry of Education, Culture, Sports, Science and Technology in Japan.

-
- ¹ N. Tajima and K. Kajita, *Sci. Tech. Adv. Mater.* **10**, 024308 (2009).
 - ² H. Seo, C. Hotta, and H. Fukuyama, *Chem. Rev.* **104**, 5005 (2004).
 - ³ A. Kobayashi, S. Katayama, and Y. Suzumura, *Sci. Tech. Adv. Mater.* **10**, 024309 (2009).
 - ⁴ H. Kino and H. Fukuyama, *J. Phys. Soc. Jpn.* **64**, 4523 (1995).
 - ⁵ H. Seo, *J. Phys. Soc. Jpn.* **69**, 805 (2000).
 - ⁶ C. Hotta, *J. Phys. Soc. Jpn.* **72**, 840 (2003).
 - ⁷ T. Takahashi, *Synth. Met.* **133-134**, 26 (2003).
 - ⁸ N. Tajima, A. Ebina-Tajima, M. Tamura, Y. Nishio, K. Kajita, *J. Phys. Soc. Jpn.* **71**, 1832 (2002).
 - ⁹ A. Kobayashi, S. Katayama, and Y. Suzumura, *J. Phys. Soc. Jpn.* **74**, 2897 (2005).
 - ¹⁰ K. Kajita, T. Ojio, H. Fujii, N. Nishio, H. Kobayashi, A. Kobayashi, R. Kato, *J. Phys. Soc. Jpn.* **61**, 23 (1992).
 - ¹¹ A. Kobayashi, S. Katayama, K. Noguchi, and Y. Suzumura, *J. Phys. Soc. Jpn.* **73**, 3135 (2004).
 - ¹² S. Katayama, A. Kobayashi, and Y. Suzumura, *J. Phys. Soc. Jpn.* **75**, 054705 (2006).
 - ¹³ R. Kondo, S. Kagoshima, and J. Harada, *Rev. Sci. Instrum.* **76**, 093902 (2005).
 - ¹⁴ H. Kino and T. Miyazaki, *J. Phys. Soc. Jpn.* **75**, 034704 (2006).
 - ¹⁵ S. Ishibashi, T. Tamura, M. Kohyama, and K. Terakura, *J. Phys. Soc. Jpn.* **75**, 015005 (2006).
 - ¹⁶ A. Kobayashi, S. Katayama, Y. Suzumura, and H. Fukuyama, *J. Phys. Soc. Jpn.* **76**, 034711 (2007).
 - ¹⁷ M.O. Goerbig, J.-N. Fuchs, G. Montambaux, and F. Piéchon, *Phys. Rev. B* **78**, 045415 (2008).
 - ¹⁸ A. Kobayashi, Y. Suzumura, and H. Fukuyama, *J. Phys. Soc. Jpn.* **77**, 064718 (2008).
 - ¹⁹ N. Tajima, S. Sugawara, R. Kato, Y. Nishio, and K. Kajita, *Phys. Rev. Lett.* **102**, 176403 (2009).
 - ²⁰ K. Morinari, T. Himura, and T. Tohyama, *J. Phys. Soc. Jpn.* **78**, 023704 (2009).
 - ²¹ A. Kobayashi, Y. Suzumura, F. Piéchon, and G. Montambaux, *Phys. Rev. B* **84**, 075450 (2011).
 - ²² T. Nishine, A. Kobayashi, and Y. Suzumura, *J. Phys. Soc. Jpn.* **79**, 114715 (2010).
 - ²³ T. Nishine, A. Kobayashi, and Y. Suzumura, *J. Phys. Soc. Jpn.* **80**, 114713 (2011).
 - ²⁴ A. Kobayashi, Y. Suzumura, H. Fukuyama, and M. O. Goerbig, *J. Phys. Soc. Jpn.* **78**, 114711 (2009).
 - ²⁵ Y. Takano, K. Hiraki, Y. Takada, H. M. Yamamoto, and T. Takahashi, *J. Phys. Soc. Jpn.* **79**, 104704 (2010).
 - ²⁶ K. Miyagawa, M. Hirayama, M. Tamura, and K. Kanoda, *J. Phys. Soc. Jpn.* **79**, 063703 (2010).
 - ²⁷ M. Hirata, Ph.D. thesis, Univ. of Tokyo, (2012)
 - ²⁸ S. Katayama, A. Kobayashi, and Y. Suzumura, *Eur. Phys. J. B* **67**, 139 (2009).
 - ²⁹ T. Mori, A. Kobayashi, Y. Sasaki, H. Kobayashi, G. Saito, and H. Inokuchi, *Chem. Lett.* 957 (1984).
 - ³⁰ T. Mori, H. Mori, and S. Tanaka, *Bull. Chem. Soc. Jpn.* **72**, 179 (1999).
 - ³¹ Y. Shimizu, A. Kobayashi, M. Ito, H. M. Yamamoto, Y. Takano, T. Takahashi, private communication.
 - ³² S. Katayama, A. Kobayashi, Y. Suzumura, private communication.

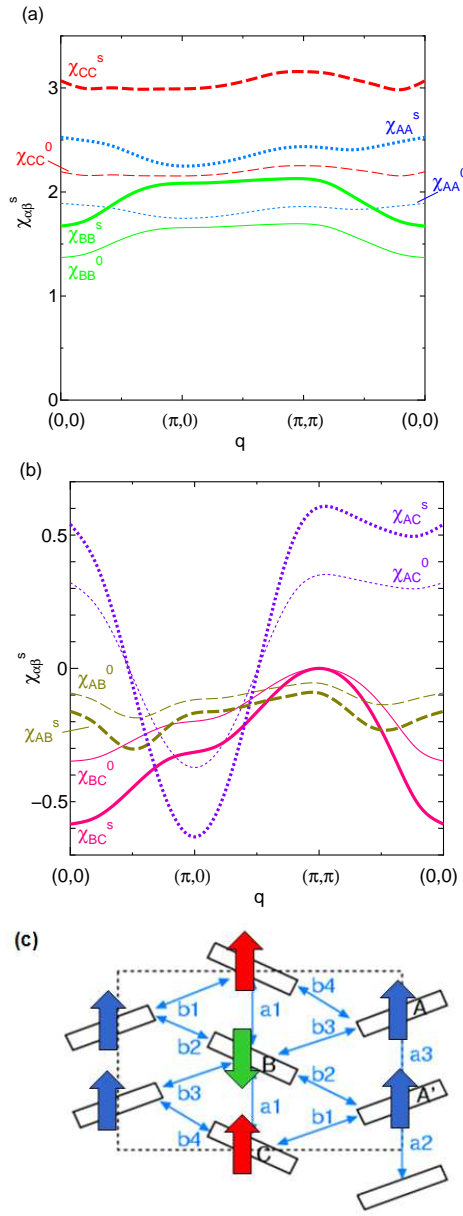


FIG. 5: (a) Momentum dependences of the diagonal components of the spin susceptibilities $\chi_{\alpha\alpha}^s$ with $U = 0.12$ (thick line) and the bare susceptibilities $\chi_{\alpha\alpha}^0$ (thin line) for $\alpha = A$ (red dashed line), B (green solid line), and C sites (blue dotted line), where $T = 0.02$ and $\omega = 0$. (b) Momentum dependences of the off-diagonal components of the spin susceptibilities $\chi_{\alpha\beta}^s$ $U = 0.12$ (thick line) and the bare susceptibilities $\chi_{\alpha\beta}^0$ (thin line) for $(\alpha, \beta) = (A, B)$ (gold dashed line), (B, C) (wine red solid line), and (A, C) sites (purple dotted line), where $T = 0.02$ and $\omega = 0$. (c) Schematic figure for pattern of the ferrimagnetic spin fluctuation. (Color Online)

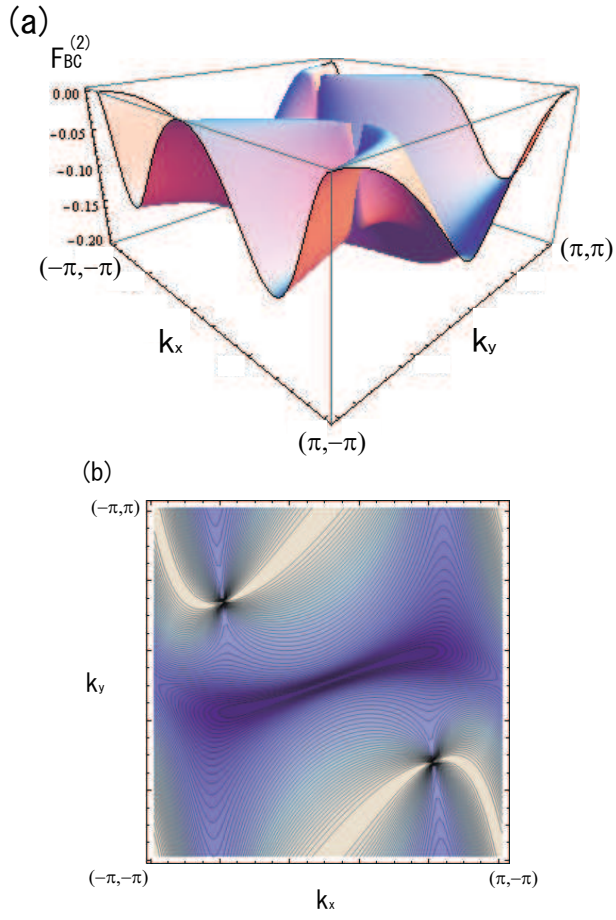


FIG. 6: (a) Momentum \mathbf{k} dependence of the form factor $F_{\text{BC}}^{(2)}(\mathbf{k}, \mathbf{0})$ for the interband fluctuation in the Brillouin zone. The contour plot corresponding to (a) is shown in (b) (Color Online)

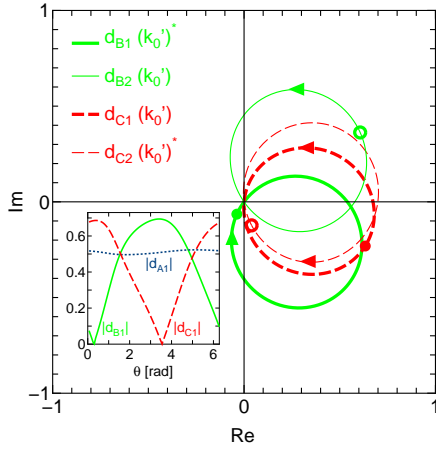


FIG. 7: Numerical results of Wave functions normalized by $d_{A\gamma}/|d_{A\gamma}|$ ($\gamma=1,2$) on the Gauss plane, for $d_{B1}(k_0')^*$ (the green thick solid circle), $d_{B2}(k_0')$ (the green thin solid circle), $d_{C1}(k_0')$ (the red thick dashed circle) and $d_{C2}(k_0')^*$ (the red thin dashed circle), where $|k_0' - k_0| = 0.05\pi$ and the angle of $k_0' - k_0$ vector from k_x -axis, θ , moves from zero to 2π . The directions where the values of wave functions move with increasing θ are represented by the arrows on the circles, and the values of wave functions at $\theta = 0$ are indicated by the filled or open small circles on the large circles. The inset shows θ -dependences of absolute values of the wave functions for the conduction band, $|d_{A1}(k_0')|$ (the blue dotted line), $|d_{B1}(k_0')|$ (the green solid line) and $|d_{C1}(k_0')|$ (the red dashed line). (Color Online)